water

MDPI

Article

# Parameter Estimation and Assessment of Infiltration Models for Madjez Ressoul Catchment, Algeria

**Asma Dahak [1], Hamouda Boutaghane [1] and Tarek Merabtene [2,*]**

[1] Soil and Hydraulics Laboratory, Badji Mokhtar University, Annaba P.O. Box 12, Algeria; asma16061991@gmail.com (A.D.); hamouda.boutaghane@univ-annaba.dz (H.B.)
[2] Department of Civil and Environmental Engineering, University of Sharjah, Sharjah P.O. Box 27272, United Arab Emirates
* Correspondence: tmerabtene@sharjah.ac.ae

**Abstract:** Evaluation and modeling of soil water infiltration are essential to all aspects of water resources management and the design of hydraulic structures. Nonetheless, research focused on experimental studies of infiltration rates in arid and semi-arid regions under unknown boundary conditions remains minimal. This paper investigates the characteristics of the spatial variability of infiltration over a semi-arid rural basin of Algeria. The experiments were conducted using a portable double-ring infiltrometer filled at an equal volume of approximately 100 L of water for each of the 25 catchment locations. Soil moisture contents at the proximity of each test location were evaluated in the laboratory as per the standard NF P94–050 protocol. The experimental results are used to produce the catchment infiltration curves using three statistically fitted infiltration models, namely Horton, Kostiakov, and Philip models. The reliability of the models was assessed using four performance criteria. The statistical regressions of the fitted models suggest that the Horton model is the most suitable to assess the infiltration rate over the catchment with mean coefficients of *Nash* = 0.963, *CC* = 0.985, *RMSE* = 1.839 (cm/h), and *Bias* = 0.241. The superiority of the Horton model suggests that the initial and final infiltration rates, primarily affected by soil type, initial soil moistures, and land cover, are important predictors of the modeling process over the Madjez Ressoul catchment. The results also infer that the applicability of other models to the different types of undeveloped soils in the study area requires advanced field investigations. This finding will support the understanding of the hydrologic processes over semi-arid basins, especially in advising crop irrigation schemes and methods and managing the recurring flood and drought over the country.

**Keywords:** Philip; Horton and Kostiakov infiltration models; saturated hydraulic conductivity; soil moisture; portable double-ring infiltrometer; Madjez Ressoul catchment; statistical criteria

check for updates

**Citation:** Dahak, A.; Boutaghane, H.; Merabtene, T. Parameter Estimation and Assessment of Infiltration Models for Madjez Ressoul Catchment, Algeria. *Water* **2022**, *14*, 1185. https://doi.org/10.3390/w14081185

Academic Editors: Md Jahangir Alam, Monzur A. Imteaz and Abdallah Shanbleh

Received: 25 January 2022
Accepted: 4 April 2022
Published: 7 April 2022



## 1. Introduction

Estimation and modeling of soil infiltration characteristics are fundamental to quantifying catchments' water storage capacity, controlling and assessing runoff processes, and planning for water-crop yield and irrigation scheduling [1]. The infiltration rate is equivalent to the saturated hydraulic conductivity [2–4]. It is a complex soil characteristic to estimate, for it depends on multiple physical and hydrologic factors, including rainfall variability [5,6], surface and deep soil properties [7–9], slope morphology [10], vegetation and land use [11], and soil moisture [12,13]. Despite the importance of these factors, infiltration is independent of the quantity and intensity of rainfall when it is less than the soil infiltration rate and is conditionally associated with the initial soil water content.

Practically, reliable information about infiltration rates is difficult to obtain without in situ experiments. The many attempts to evaluate infiltration rates using permeability values from the laboratory have achieved poor results, even if combined with mass balance equations. In this context, ref. [14] reported that the prediction of infiltration rates with an

infiltrometer, for catchments in central Florida, was more accurate than those obtained from laboratory permeability values. Further challenges are the inclusion of soil heterogeneity, including land use and soil vegetation covers in the spatio-temporal scale evaluation of infiltration rates (e.g., [15–18]). Owing importance of infiltration in hydrological modeling, ref. [19] studied how runoff was affected by soil properties and anthropogenic changes and concluded that modeling rainfall independently from infiltration and antecedent or initial soil moisture is complex and remains crucial in choosing the calibration strategy. Additionally, early and recent efforts to evaluate infiltration directly from field measurements indicate that variation among infiltration rates depends on slope gradients, surface characteristics, and geomorphologic angle [20,21].

Many authors assert that establishing tailored infiltration models based on regression analysis would be the simplest and most effective method to evaluate infiltration rates [22–24]. This is generally achieved by fitting linearly or nonlinearly field experiment measurements to well-established and widely accepted theoretical models of infiltration. Consequently, distribution graphs and parameters can be obtained based on multivariate statistical and geostatistical analyses [25]. Such studies have assessed and compared the reliability and effectiveness of new and traditional infiltration models based on standard statistical criteria [26–29]. These studies confirm that infiltration time is the most influential parameter for estimating infiltration rate [30]. Reciprocally, studies over arid and semi-arid regions have agreed that empirical and semi-empirical models have found a more significant ground for applications [31–33].

The Horton model was among the earliest infiltration models introduced based on the concept of infiltration-excess overland flow as a runoff-generation process [34]. Researchers proposed numerous modifications to the Horton model to account for moisture storage in lower soil [35] and intermittent rainfall during short events in dry seasons [36], as well as to calibrate it for large catchment areas [37]. Despite criticisms regarding the interrelations between the infiltration rate, amount of rainfall, and maximum infiltration capacity during a storm event [38–40], the Horton model is still widely adopted. It provides a generally good agreement to in situ data and can reflect the physical basics of soil as three of its parameters are measured experimentally. Reliable calibration of the model parameters determines the accuracy of the simulated infiltration rate of the models mentioned above (e.g., [41–44]). Studies also showed that using a double-ring infiltrometer for base experiments is preferred over other methods [45,46] applied three empirical infiltration models, including the Horton model, to assess the efficiency of wastewater infiltration for managing the problem of water scarcity and maintaining hydraulic infrastructure in Iranian catchments. Similarly, ref. [47] examined water retention and soil capacity using a double-ring infiltrometer and several infiltration models to improve the problem of desertification in a part of China, including for crop irrigation scheduling.

The reliability of traditional empirical and semi-empirical infiltration models was a subject of many investigations [48–51]. A particular focus has been given to the variability of infiltration rates as a function of changes in land use, as it can influence the amount of runoff and increase soil degradation. The authors of [52] found that the Kostiakov model had a higher accuracy with the lowest parameter uncertainty for predicting infiltration behavior over an Indian catchment compared to the Philip model. In contrast, ref. [53] concluded that the Philip model was more suitable than the Kostiakov model for predicting water infiltration within the inspected Nigerian humid forest catchment. On the other hand, ref. [54] stated that the choice and reliability of any infiltration model depends on the geological soil context. Their work concluded that the Kostiakov model was more reliable for predicting infiltration rates in soils derived from sandstone and alluvial soils. In contrast, the Philip model performed better for coastal plain sands. Similar conclusions with regard to the Kostiakov model have been obtained at a global scale [55], for example, in Iran [56,57], India [58], China [59], and Nigeria [60].

The authors of [61] concluded that the simulated cumulative infiltrations on sandy soil using the Kostiakov, Philip, and Horton models performed equally well and were close

to field measurements. Conversely, when comparing the Philip model with Kostiakov and Horton models, ref. [27] found that the Philip model failed to provide the best simulation of infiltration data. Nonetheless, they agreed that these three models are appropriate to simulate the cumulative infiltration and depth based on field measurements. The infiltration models' suitability and prediction accuracy are significantly influenced by the site conditions, as these models do not consider the variation of the initial water content. For instance, refs. [62,63] reported that if the aim was to estimate surface runoff to optimize irrigation projects, then the Kostiakov model is preferable to the Philip model.

The few studies on infiltration rates in Algeria were based on laboratory tests using in situ extracted soil samples [64]. The author of [65] developed a numerical model to assess infiltration in unsaturated dry soil from lab measurements using "flow line temperature" software as a black-box model. The authors of [66] focused on evaluating lateral and vertical hydraulic conductivity on soil profile or total infiltration flux on an agricultural parcel. The lack of studies highlights the practical need to characterize infiltration over semi-arid Algerian catchments. It is the first study to investigate the optimality of the models mentioned above based on in situ measurements from different types of soils over the catchment.

The most approved and extensively used in situ infiltration measurement is the double-ring infiltrometer. Numerous studies [67–71] concluded that it practically produces sound measurements due to its performance in reducing the effect of lateral flow. The authors of [61,71], to cite only a few, showed that the reliability to assess the robustness of empirical and semi-empirical infiltration models relies on the efficiency of the measuring method and scale of the double-ring infiltrometer. The authors of [72] pointed out that rings with large diameters (i.e., no less than 72 in for the inner ring and 216 in for the outer ring) are more robust in determining the average infiltration rate. They usually provide more accurate data for any soil and are more relevant for large-sized particles of soil.

## 2. Materials and Methods

### 2.1. Study Area

The Madjez Ressoul catchment (Figure 1) stretches southwest over a hydraulic length of about 25 km along its two main rivers, the Oued Mouya and Oued Guis. The catchment is characterized by its semi-arid climate, typically hot during summers and cold in winters, with an annual average rainfall of 635.87 mm. The daily rainfall is intermittent and can reach over 105 mm/day, whereas evapotranspiration can be as high as 7 mm/day. The catchment relief shows substantial topographic variation with elevations ranging between 70 and 930 m (evaluated from a 30 m ASTER elevation model using ArcGIS), covering 9813 hectares of extensive soil textures and heterogeneous geological formations.

For generations, agriculture in the Madjez Ressoul catchment has been the most vital social and economic activity for the local population. Agricultural activities are supported by seven hill reservoirs distributed over the entire catchment. Agricultural land represents about 83.3% of the total catchment area, for which cropped land accounts for 56.7%, irrigated land 2.7%, and forest land 23.9%. The land cover has remained one of the country's rare natural catchments, supported by significant agriculture activities over the catchment, including dry farming, community gardening, polyculture, and arboriculture. Sedimentary rocks (i.e., clay-limestone and sandstone) and bare soils are naturally distributed over the catchment (Figure 1). The selected catchment belongs to the larger Algerian Seybous watershed and holds a national strategic position for regional water supply and irrigation.

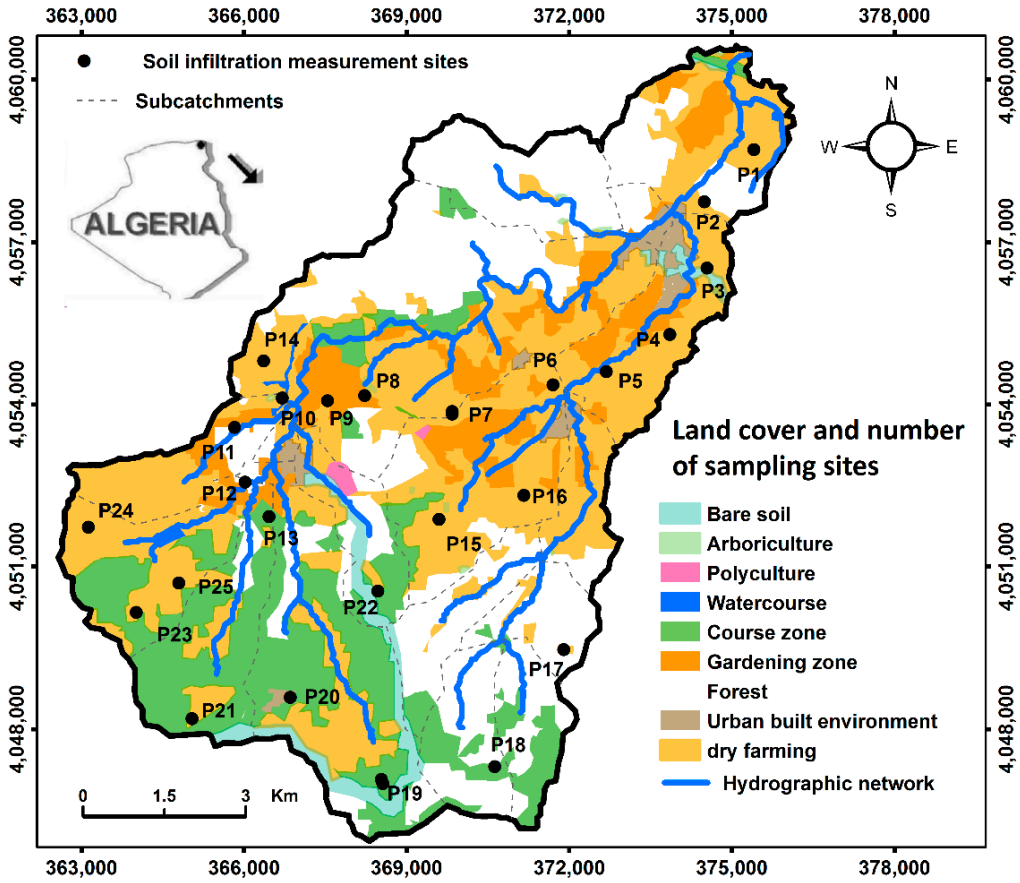


**Figure 1.** Land cover and hydrographic network of Madjez Ressoul catchment.

### *2.2. Field Measurements and Measuring Methods*

Measurements were primarily conducted at parcel levels to create a representative areal distribution of infiltration rates over the catchment. The catchment was divided into several sub-catchments, delineated according to the drainage patterns of the catchment. Five test locations (on average) were selected within each sub-catchment to comprise the largest and most dominant soil types. However, due to the complex natural reliefs, especially in high-land areas, only 25 locations were the subject of infiltration measurements (see Figure 2). The sites' accessibility and the feasibility of experiments at the selected locations were certified using the expertise of a local geologist. The Universal Transverse Mercator (UTM) coordinates for the sampling locations are given in Table 1.

Performing experiments on a sub-catchment scale, particularly in arid and semi-arid areas, is difficult due to the prevailing micro-hydrology and flow direction effects that may act in all directions and affect macropores [73]. The experiment used a standard, locally made double-ring infiltrometer with inner and outer rings of diameters 30 cm and 60 cm, respectively (Figure 3). The outer ring is used to control the variation of the transmitted water into the soil and acts as a vertical fluid barrier to control undesired lateral flows. Both rings were equally inserted in situ at 5 cm depth using a driving plate and impact-absorbing hammer. Due to the unavailability of an automated floater, a measuring ruler was installed onto the inner ring. Water in both rings was steadily maintained at the same level. At the start of each experiment, initial infiltration rates over time were recorded. After that, repeated records of infiltration depth were performed regularly every 2 min until a steady curve of infiltration rate was reached. Depending on the soil contexts in the sub-catchment, each measurement lasted from 1 to 4.5 h. The results of initial and final infiltration levels are summarized in Table 2.

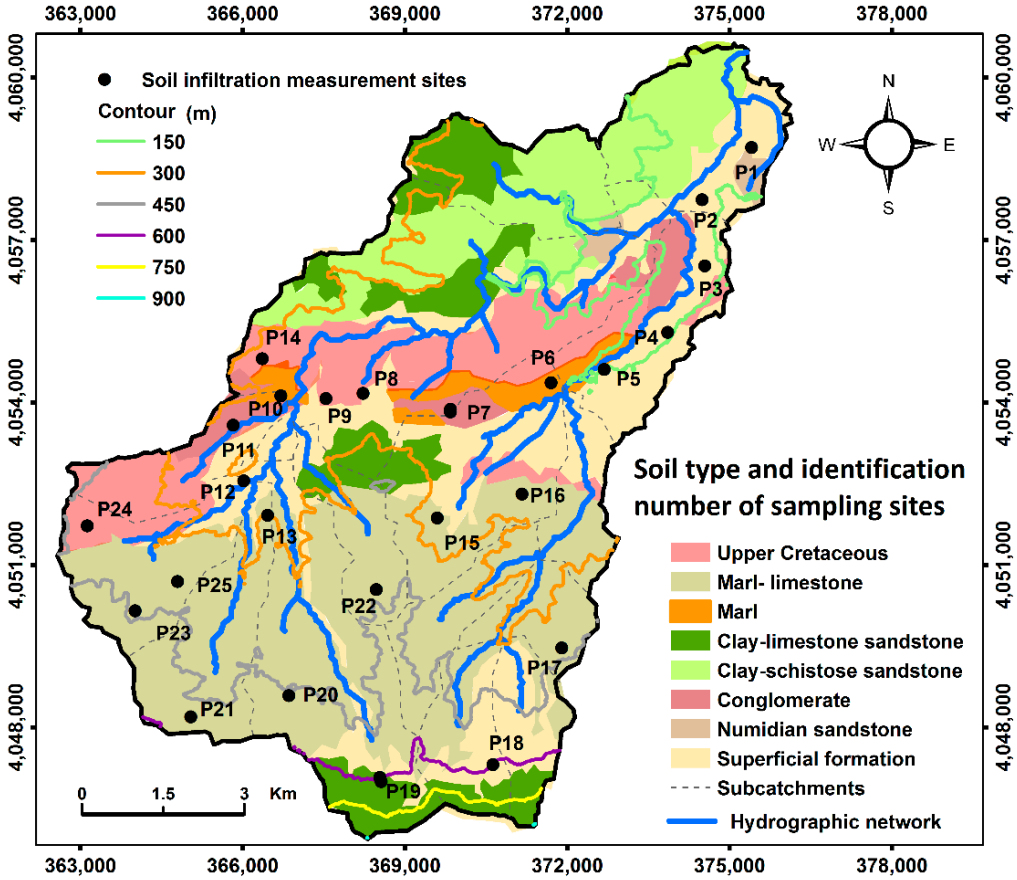


**Figure 2.** Type of soils and network of measurement points over Madjez Ressoul catchment.


**Figure 3.** Experimental double rings infiltrometer.

**Table 1.** UTM Coordinate system of measurement locations in Madjez Ressoul catchment.

| N° | X (m) | Y (m) | N° | X (m) | Y (m) |
|---|---|---|---|---|---|
| P1 | 375,425.62 | 4,058,710.17 | P14 | 366,337.18 | 4,054,866.19 |
| P2 | 374,496.25 | 4,057,723.53 | P15 | 369,589.50 | 4,051,912.45 |
| P3 | 374,533.68 | 4,056,506.43 | P16 | 371,186.40 | 4,052,366.52 |
| P4 | 373,893.76 | 4,055,315.90 | P17 | 371,897.50 | 4,049,519.69 |
| P5 | 372,720.30 | 4,054,656.09 | P18 | 370,680.00 | 4,047,361.72 |
| P6 | 371,720.73 | 4,054,348.72 | P19 | 368,502.03 | 4,047,109.89 |
| P7 | 369,870.38 | 4,053,866.53 | P20 | 366,831.31 | 4,048,601.47 |
| P8 | 368,255.99 | 4,054,208.03 | P21 | 365,040.89 | 4,048,188.93 |
| P9 | 367,492.01 | 4,054,096.72 | P22 | 368,495.87 | 4,050,579.35 |
| P10 | 366,726.87 | 4,054,144.07 | P23 | 363,989.19 | 4,050,114.83 |
| P11 | 365,854.40 | 4,053,583.85 | P24 | 363,162.02 | 4,051,752.15 |
| P12 | 366,080.29 | 4,052,571.78 | P25 | 364,839.14 | 4,050,714.70 |
| P13 | 366,465.12 | 4,051,965.49 | | | |

**Table 2.** Initial and final infiltration rates for Madjez Ressoul catchment.

| N° | Initial Infiltration Rate $f_0$ at $t$ = 2 min [cm/min] | Final Infiltration Rate $f_c$ min [cm/min] |
|---|---|---|
| P1 | 1 | 0.6 |
| P2 | 2.5 | 0.1 |
| P3 | 1 | 0.2 |
| P4 | 1 | 0.1 |
| P5 | 0.9 | 0.1 |
| P6 | 0.5 | 0.1 |
| P7 | 1.1 | 0.1 |
| P8 | 1.3 | 0.2 |
| P9 | 1.1 | 0.1 |
| P10 | 1.2 | 0.1 |
| P11 | 1 | 0.2 |
| P12 | 1.2 | 0.2 |
| P13 | 1 | 0.1 |
| P14 | 1.3 | 0.1 |
| P15 | 1.5 | 0.1 |
| P16 | 1 | 0.1 |
| P17 | 1.2 | 0.1 |
| P18 | 1 | 0.1 |
| P19 | 1.1 | 0.1 |
| P20 | 0.5 | 0.1 |
| P21 | 1.1 | 0.1 |
| P22 | 1 | 0.1 |
| P23 | 1 | 0.2 |
| P24 | 1.1 | 0.1 |
| P25 | 1.5 | 0.1 |

The initial soil moisture content was evaluated from a soil sample collected in the vicinity of each measurement site, according to the principles of the standard NF P94–050 elaborated in 1995, also referred to as the oven drying procedure. Under normal conditions (i.e., natural soil conditions after removing surface vegetation and avoiding plowed or contaminated fields by fertilizer), soil samples (15 cm deep) were collected in small air-tight containers before the experiment began to obtain their mass, applying a rigorous weighing balance. The collected quantity of the sample depends upon the maximum size of the particles and the wetness degree of the soil. A total of 100 g of each soil sample was then dried in an oven at a temperature of 105° C for 24 h. Dried soils are allowed to cool for 30–60 min before weighing. The temperature range was selected to be suitable for all samples: a value higher than 105° C may cause loss of chemically bound structural water,

and a temperature lower than this may not cause complete water evaporation. The findings of initial water contents at the sampling sites are shown in Table 3.

**Table 3.** Initial soil moisture contents in percent.

| N° | Day | Moisture Content (%) | N° | Day | Moisture Content (%) |
|---|---|---|---|---|---|
| P1 | 14 April 2019 | 21.21 | P14 | 28 April 2019 | 23.00 |
| P2 | 15 April 2019 | 40.06 | P15 | 6 May 2019 | 13.90 |
| P3 | 19 April 2019 | 26.58 | P16 | 6 May 2019 | 21.21 |
| P4 | 17 April 2019 | 29.03 | P17 | 7 May 2019 | 16.69 |
| P5 | 20 April 2019 | 25.79 | P18 | 7 May 2019 | 9.89 |
| P6 | 20 April 2019 | 14.81 | P19 | 9 May 2019 | 19.33 |
| P7 | 22 April 2019 | 8.58 | P20 | 9 May 2019 | 19.76 |
| P8 | 22 April 2019 | 12.11 | P21 | 11 May 2019 | 24.69 |
| P9 | 23 April 2019 | 13.77 | P22 | 11 May 2019 | 14.16 |
| P10 | 23 April 2019 | 16.82 | P23 | 12 May 2019 | 28.53 |
| P11 | 25 April 2019 | 14.81 | P24 | 12 May 2019 | 16.69 |
| P12 | 25 April 2019 | 12.11 | P25 | 13 May 2019 | 13.38 |
| P13 | 28 April 2019 | 20.77 | | | |

### *2.3. Parametrization of Infiltration Models for Madjez Ressoul Catchment*

As mentioned earlier, there is an ongoing debate on the most efficient models for evaluating in situ infiltration rates. Only ample and accurate field measurements could be decisive on the adequacy of one method over another. This study analyses the measured infiltration data to identify the calibration parameters of the three most commonly used infiltration models, namely the Horton, Kostiakov, and Philip models.

The Horton model [74] is a semi-empirical model used to quantify infiltration rate as an exponential decay function, assuming saturation conditions at the soil surface over time (Equation (1)). It is among the most widely tested models worldwide for engineering purposes (e.g., [75]). It is mathematically expressed as:

$$f(t) = f_c + (f_0 - f_c)e^{-kt} \tag{1}$$

where $f(t)$ is the infiltration rate at time $t$ in [LT$^{-1}$], $f_c$ is the final constant infiltration capacity in [LT$^{-1}$], $f_0$ is the initial infiltration capacity at time $t = 0$ in [LT$^{-1}$], and $k$ in [T$^{-1}$] is the decay rate constant.

The Kostiakov model [76] was first proposed for the analysis of infiltration in irrigation projects. The empirical model (Equation (2)) tends to estimate infiltration rates as a decay function over time, assuming that limit of infiltration will converge to zero as time converges to infinity. It is mathematically expressed as:

$$f(t) = At^{-B} \tag{2}$$

where $f(t)$ is the infiltration rate at time $t$ in [LT$^{-1}$], and $A$ and $B$ are the unknown equation parameters representing soil infiltration characteristics, with $A$ being a measure of the initial rate of infiltration and structural condition of the soil, and $B$ an index of soil structural stability.

The Philip Two-term Model [77] is a physical infiltration model (Equation (3)). It was initially developed for uniform soil, where the decay infiltration rate depends on the analysis of penetrated water and the soil properties. It is mathematically expressed as:

$$f(t) = \frac{1}{2}St^{-0.5} + K \tag{3}$$

where $f(t)$ is the infiltration rate at time $t$ in [LT$^{-1}$], $S$ in [LT$^{-0.5}$] is the sorptivity parameter reflecting the soil absorption capacity as a function of the soil matric forces during the

initial phases of the infiltration process, and $K$ in [$LT^{-1}$] is a constant proportional to the hydraulic conductivity.

### 2.4. Model Calibration and Assessment of Model Parameters

The parameters of the models were evaluated for each test location to establish a general model for the Madjez Ressoul catchment by capturing similarities among the sub-catchments. The calibration of the models was based on least square analysis. The method estimates the minimum sum of squared residuals ($SSE_i$) between observed and simulated data using an objective equation of the form shown in (Equation (4)). Adjusted distributions of measured and calculated infiltration rates require routine assessment of parameters according to the regression lines to quantify the linear trend. After treatments, these linear fittings were taken as the first testing of observed data to consider the initial input variables of each infiltration model. Hence, parameters with the highest correlation coefficients are used to gain consistently better predictions. In the second stage, the following optimization step was carried out by comparing residuals between observed and simulated infiltration data.

$$SSE_i = \sum_{j=1}^{N} (f_{Obs}(i,j) - f_{sim}(i,j))^2 \tag{4}$$

The models' performance and the parameters' goodness of fit were assessed using four statistical criteria: *Nash*–Sutcliffe (*Nash*), Pearson correlation coefficient (*CC*), Root mean square error (*RMSE*), and *Bias* estimate.

The *Nash*–Sutcliffe coefficient (*Nash*) (Equation (5)) is one of the most used criteria in hydrology despite its known drawback (neglecting lower infiltration rates, while larger ones are overestimated considering that residuals are calculated as squared values). *Nash* values range from 0–1, where a value close to 1 indicates a better fit. Practically the *Nash* values are highly associated with the coefficient of determination ($R^2$).

$$Nash_i = 1 - \frac{\sum_{j=1}^{N} (f_{Obs}(i,j) - f_{sim}(i,j))^2}{\sum_{j=1}^{N} (f_{Obs}(i,j) - \overline{f_{Obs}})^2} \tag{5}$$

Pearson's correlation coefficient (*CC*) is based on the method of covariance (Equation (6)). It is used as a measure of the strength of linearity association between observed and simulated infiltration variables. Its values range between −1 and +1, where a value of +1 indicates a perfect positive correlation with strength equal to its absolute value.

$$CC_i = \frac{N(\sum f_{Obs}(i,j) \times f_{sim}(i,j)) - (\sum f_{Obs}(i,j))(\sum f_{sim}(i,j))}{\sqrt{[n(\sum f_{Obs}(i,j)^2) - (\sum f_{Obs}(i,j))^2][n(\sum f_{sim}(i,j)^2) - (\sum f_{sim}(i,j))^2]}} \tag{6}$$

The Root mean square error (*RMSE*) is a standard method commonly used as a correspondence index between observed and simulated data. *RMSE* (Equation (7)) is always positive without a defined range or thresholds, but generally, the smaller the value, the better.

$$RMSE_i = \sqrt{\frac{\sum_{j=1}^{N} (f_{Obs}(i,j) - f_{sim}(i,j))^2}{N}} \tag{7}$$

*Bias* analysis (*Bias*) provides a numerical approximation of the magnitude of uncertainty arising from error estimates. *Bias* estimate (Equation (8)) is evaluated by dividing the difference between observed and simulated data to the number of estimates. A value of zero indicates that the estimator is unbiased.

$$Bias_i = \frac{\sum_{j=1}^{N} (f_{Obs}(i,j) - f_{sim}(i,j))}{N} \tag{8}$$

where, for the above equations, $i$ is the index of the sampling sites, $j$ is the index of recorded or simulated infiltration at time $t$, $N$ the total number of recorded measurements, $f_{Obs}(i,j)$ is the $j$th observed (i.e., recorded) infiltration rate at site $i$ in ($LT^{-1}$), $\overline{f_{\text{Obs}}}(i,j)$ is the mean observed infiltration rate in ($LT^{-1}$), $f_{sim}(i,j)$ is the simulated infiltration rates in ($LT^{-1}$).

## 3. Results

### *3.1. Effect of Soil Texture and Soil Moisture on Infiltration Rates*

The infiltration rates spread over five significant processes (Figure 4), despite distinctive variations in soil types and altitudes of the measurement sites. A mean initial infiltration rate of 32 cm/h (i.e., statistical mode 30 cm/h) was reached after nearly 2 min of operation. The lowest measured infiltration rates were at site 20 (Soil: marl-limestone; Altitude: ~400 m) and site 6 (soil: superficial formation; Altitude: ~200 m), with only half of the mean value. The two other extremes are sites 15 (Altitude: ~250 m) and P25 (Altitude: ~400 m), located within the same soil formation (i.e., marl-limestone), with 40% higher rates after 2 min. Saturation thresholds varied from 0.1–3 cm/h (i.e., with an average, median and mode of nearly 1.5 cm/h). These variations within the same soil formations also occurred within the three most predominant soils, namely, marl-limestone (0.3–3 cm/h), marl soil (0.1–2 cm/h), and superficial formations (0.3–2.5 cm/h). Different saturation limits are encountered within the same soil formations. For example, within the marl-limestone formation, sites 15, 23, and 25, the limit was 1.5 cm/h. In comparison, at sites 21 and 22, the limit was 0.3 cm/h. Whereas at sampling sites 6 and 20, the initial infiltration rates were very low (i.e., 0.5 cm/h compared to the statistical mean, median, and mode of 1). In contrast, sites within marl and superficial formations had no comparable values. These findings reveal the influence of the soil properties over the Madjez Ressoul catchment dominated by sandy stone, organic sedimentary Cretaceous, and limestone. The initial soil moisture is another factor that could have influenced the variations of initial and final infiltration rates within the same soil texture. For instance, at sampling site 2, the initial soil moisture content and initial infiltration rate were exceptionally high compared to neighboring sites 3 and 4 within the same soil. Unfortunately, the experimental setting asserts that the hydraulic relationship between soil characteristics and infiltrated rates is complex and cannot be fully developed using the chosen infiltration equations even for soils within the same structure.

As mentioned earlier in Section 2.2, the percentages of initial water contents at the sampling sites were determined for the existing soil conditions before each experiment (Table 3). As shown in Figure 5, the response times to reach the saturation limit varied from 0.4 h at site 2 to 3.6 h at site 7, with, respectively, the highest and lowest initial moisture contents of 40.06% and 8.58% (see Table 3). In contrast, a longer saturation time was observed at site 21 (of 4.3 h), characterized by a relatively high initial water content of 24.69% and an estimated infiltration capacity of 33 cm/h. It is also remarkable to notice the differences in infiltration responses at sites 15, 17, 21, and 22 of dominant sandy soil type. These sites exhibited quicker water movements than site 19 of dominant clay soil of tiny pores structure that may restrict percolation and increase overland flow.

The observed initial infiltration rates were similar for sites 1, 3, 4, 13, 18, 22, and 23 with $f_0$ = 30 cm/h, and sites 7, 19, 21, and 24 with $f_0$ = 33 cm/h, and sites 25 and 15 with $f_0$ = 45 cm/h. Thus, initial soil moistures show dry conditions for sites with high infiltration capacities and humid conditions for sites with low infiltration capacities. It is interesting to note the distinctive responses of sites 7 and 11, which are naturally located within conglomerate formations. According to [78], the texture of sedimentary rock formations, with interconnectedness between the large overall grain size, contributes to its permeability and allows the soil to hold less water.

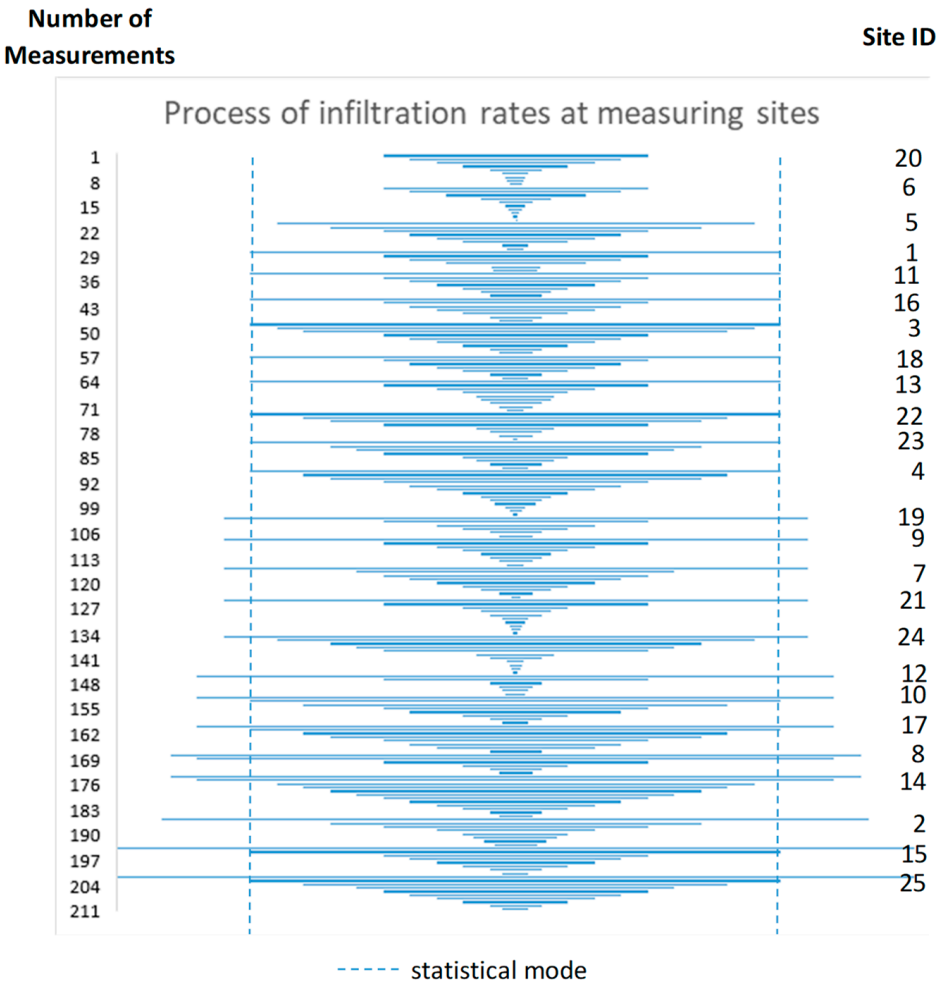


**Figure 4.** Progress of the process of infiltration rates at measuring stations (number to the left).

### *3.2. Performance Evaluation of Infiltration Models for Predicting Infiltration Rates*

The general tendency of the simulated values by the three models compared to the overall distribution of infiltration measurements is depicted in Figure 6a,b. Although not all models performed equally at all points compared to the measured values, the overall Pearson correlation coefficients between the observed and simulated values by the Horton, Kostiakov, and Philip models were statically significant with *CC* values of 0.985, 0.958, and 0.968, respectively.

The reliability of the three models can be further assessed through the cross-correlations between the experimental and simulated infiltrations rates. The inter-model cross-correlations, presented in Figure 7 (at Lag $k$ = 2 and using a 95% confidence interval shown as dashed lines), assert that the overall performances of the three models are equally good. Nonetheless, it is worth mentioning that the weakest inter-model cross-correlation was between Kostiakov and Horton, with *CC* = 0.88. Likewise, the maximum and minimum infiltration rates vary widely between models, ranging from 39.64–0.44 (cm/h), 46.98–1.28 (cm/h), and 44.05–1.53 (cm/h) for the Horton, Kostiakov, and Philip models, respectively. The three models' parameters were calibrated to observed data using linear and nonlinear regression methods.

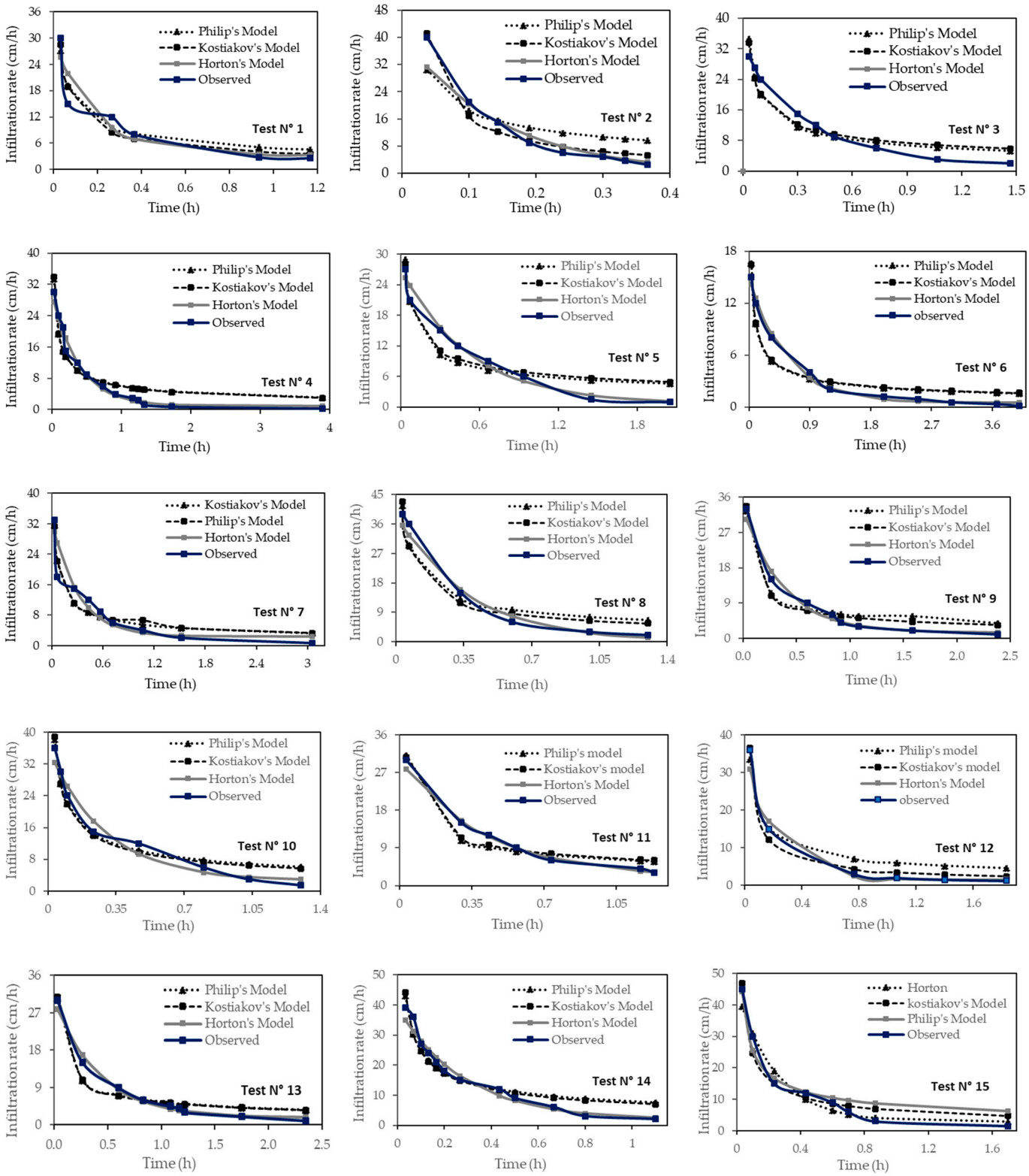


**Figure 5.** *Cont.*

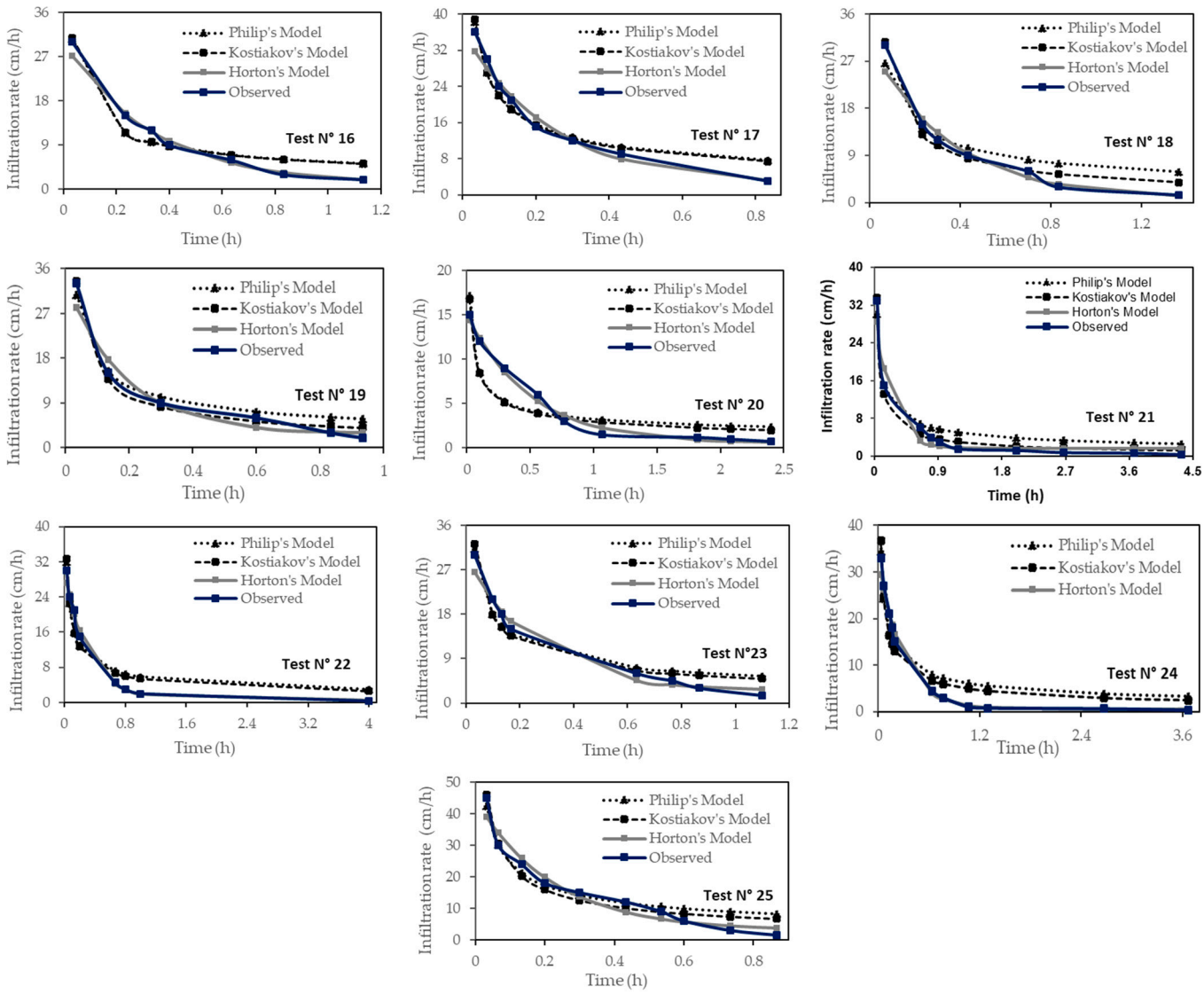


**Figure 5.** Inter-comparison of field infiltration rates from different models for Madjez Ressoul catchment.

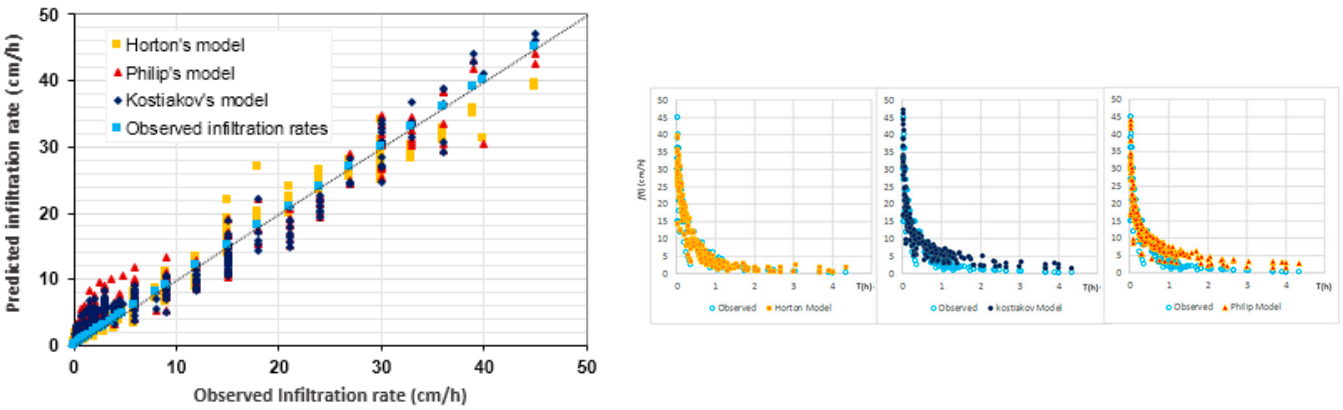


(**a**) (**b**)

**Figure 6.** (**a**) Overall linear dependency of observed versus simulated infiltration rates at all site locations. (**b**) Overall behavior of the models' simulations compared to the overall field measurements.

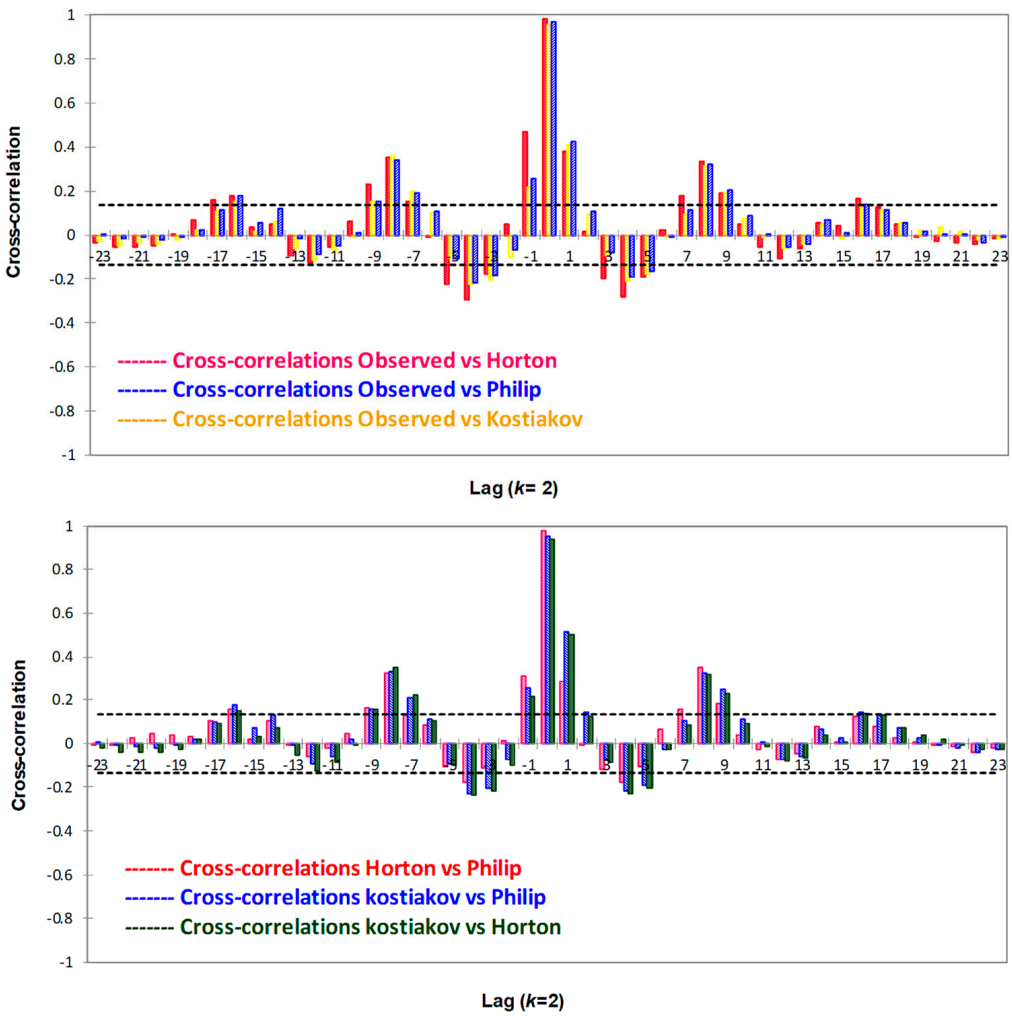


**Figure 7.** Observed versus models and Inter-models cross-correlations.

Figure 8 shows the variation of the models' parameters evaluated for each test location. Kostiakov parameter ***B*** varies between 0.425 and 0.6 for most sites except site 2, where the maximum value of 0.89 was obtained. Similarly, Philip parameter ***K*** varies for most sites between 0.012 and 0.038 cm/h except for sites 5, 11, and 20, which have significantly higher values of 0.99, 0.743, and 0.841 cm/h, respectively. The results obtained for Kostiakov parameters ***A*** and ***B*** agree with earlier studies despite the arguments of [79] that the range of parameter ***B*** can be mathematically higher than one. Higher *B* values were obtained for steeper slopes and for a more significant rate of decline in soil infiltration, as shown for sites 12, 15, 21, and 24. The other asserted drawback from the results of this study is the weakness of the Kostiakov model for converging toward a final steady infiltration rate ($f_c$).

As shown in Figure 8, Horton parameter *K*'s values range from 1.795 ($h^{-1}$) at site 6 to 6.744 ($h^{-1}$) at site 2, and the Kostiakov parameter *A* ranges from 2.174 at site 2 to 7.29 at site 14. Nonetheless, several sites exhibit similar values. The Philip parameter *S* (i.e., soil sorptivity) has significantly higher variation, ranging from 4.854 cm/$h^{-0.5}$ at site 20 to 6.17 cm/$h^{-0.5}$ at site 6, in contrast to nearly 16 cm/$h^{-0.5}$ at sites 14, 15, and 25. Nonetheless, 12 out of 25 sites exhibited equivalent sorptivity values ranging between $S$ = 11 cm/$h^{-0.5}$ and $S$ = 13 cm/$h^{-0.5}$. Table 4 summarizes the best-estimated parameters for the three infiltration models at each test location.

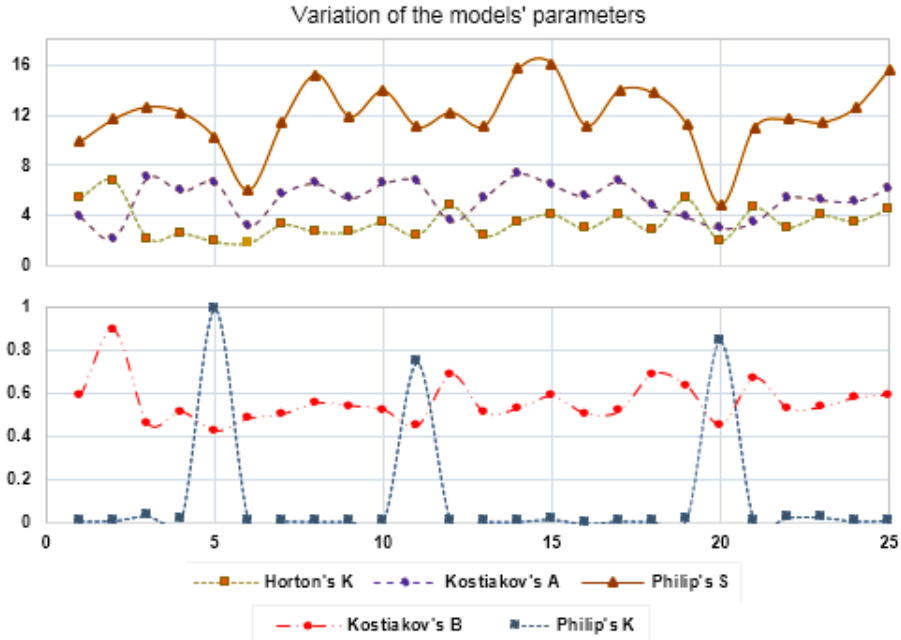


**Figure 8.** Variation of the three models' parameters and infiltration rates over Medjaz Ressoul catchment.

**Table 4.** Calculated parameters of infiltration models.

| N° | Horton's Model | Kostiakov's Model | | Philip's Model | |
|---|---|---|---|---|---|
| | $k$ (h$^{-1}$) | $A$ | $B$ | $S$ (cm/h$^{0.5}$) | $K$(cm/h) |
| P1 | 5.403 | 3.875 | 0.586 | 9.893 | 0.012 |
| P2 | 6.744 | 2.174 | 0.890 | 11.688 | 0.014 |
| P3 | 2.18 | 6.975 | 0.462 | 12.647 | 0.0379 |
| P4 | 2.576 | 5.920 | 0.514 | 12.216 | 0.020 |
| P5 | 1.897 | 6.625 | 0.425 | 10.211 | 0.990 |
| P6 | 1.795 | 3.182 | 0.483 | 6.070 | 0.012 |
| P7 | 3.243 | 5.695 | 0.503 | 11.429 | 0.012 |
| P8 | 2.682 | 6.527 | 0.554 | 15.218 | 0.010 |
| P9 | 2.643 | 5.334 | 0.542 | 11.885 | 0.010 |
| P10 | 3.411 | 6.529 | 0.524 | 13.930 | 0.010 |
| P11 | 2.402 | 6.671 | 0.449 | 11.077 | 0.743 |
| P12 | 4.774 | 3.529 | 0.687 | 12.218 | 0.010 |
| P13 | 2.368 | 5.434 | 0.510 | 11.156 | 0.010 |
| P14 | 3.504 | 7.290 | 0.530 | 15.682 | 0.010 |
| P15 | 4.080 | 6.403 | 0.586 | 16.078 | 0.020 |
| P16 | 2.939 | 5.512 | 0.506 | 11.182 | 0/013 |
| P17 | 4.037 | 6.678 | 0.517 | 13.960 | 0.012 |
| P18 | 2.786 | 4.747 | 0.689 | 13.748 | 0.010 |
| P19 | 5.320 | 3.855 | 0.634 | 11.217 | 0.020 |
| P20 | 1.987 | 2.975 | 0.454 | 4.854 | 0.841 |
| P21 | 4.611 | 3.420 | 0.671 | 11.003 | 0.010 |
| P22 | 3.055 | 5.371 | 0.531 | 11.668 | 0.030 |
| P23 | 4.000 | 5.209 | 0.536 | 11.414 | 0.030 |
| P24 | 3.517 | 5.110 | 0.579 | 12.553 | 0.012 |
| P25 | 4.537 | 6.145 | 0.593 | 15.581 | 0.015 |

The performances of the three models for predicting infiltration rates at site locations were validated according to the four performance criteria (i.e., *Nash*–Sutcliffe (*Nash*), Pearson correlation coefficient (*CC*), Root mean square error (*RMSE*), and *Bias*). The variations of the four statistical coefficients for all sites are depicted in Figure 9.

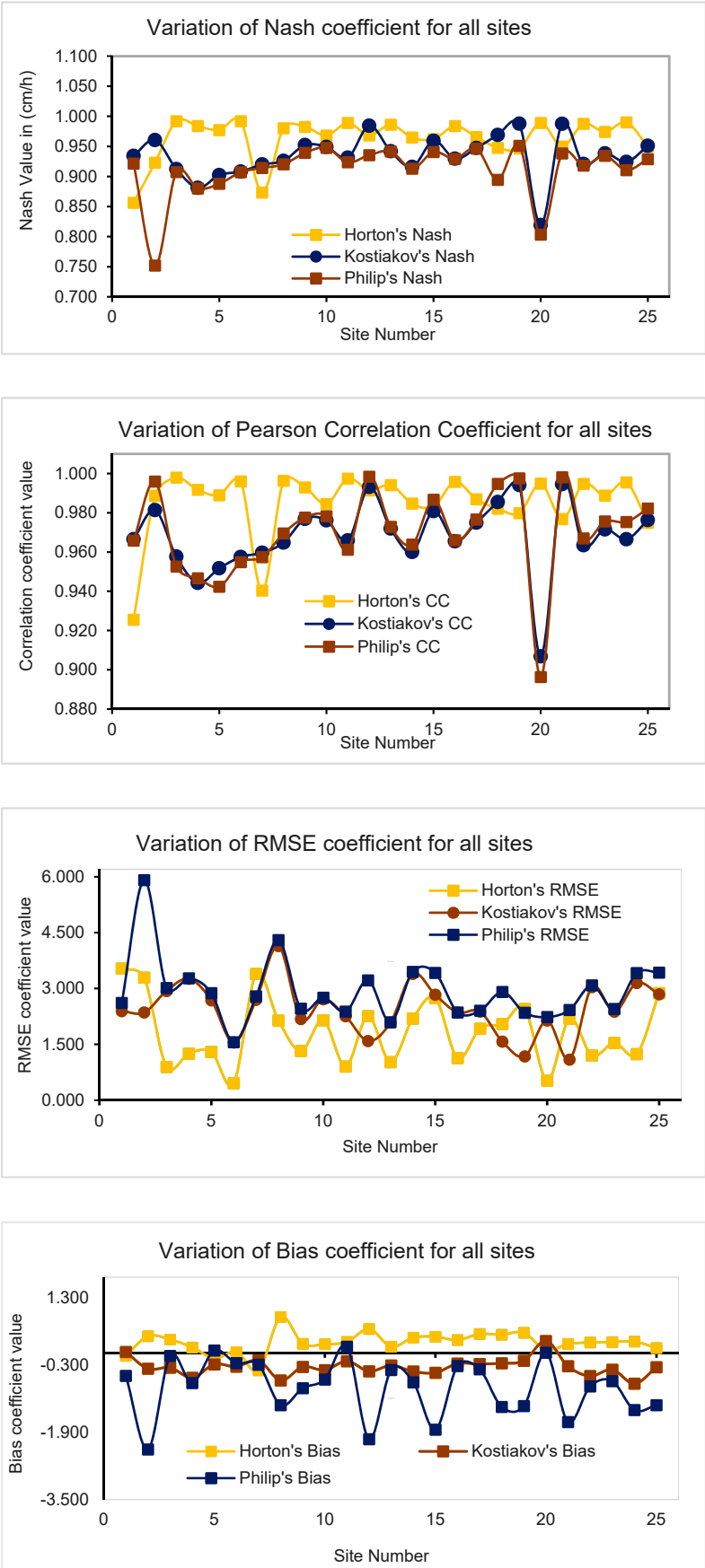


**Figure 9.** Validation of estimated parameters according to the variation of statistical measures.

Among the models, the Horton model exhibited the best fitting performance with a higher *Nash* and correlation coefficient and the least *RMSE* and *Bias*. Consequently, the performance of the Horton model is statistically significant for the 25 sites, with *Nash* values ranging from 0.856–0923 at sites 1, 2, and 7 and 0.947–0.992 for all other sites. The parameter *CC* ranged from 0.925–0.940 at sites 1 and 7 to 0.975–0.998 for all other sites. The *RMSE* varied from 2.743–3.536 at sites 1, 2, 7, 15, and 25 to 0.457–2.450 for all other sites. In contrast, the *Bias* estimate ranged from −0.418 at site 7 to 0.852 at site 8. The coherence of all tests supports the superior performance of the Horton model for modeling infiltration rates at the Madjez Ressoul catchment. The superiority of the Horton model suggests that soil moisture and the initial and final infiltration rates are dominant factors in modeling the infiltration processes over the Madjez Ressoul catchment. The results also infer the importance of soil properties, soil hydraulic parameters, and the infiltration measurement method as influential parameters and constraints in modeling infiltration at specific sites. Thus, the applicability of other models to the different types of undeveloped soils in the study area requires advanced field investigations. As semi-empirical models lack definite physical meaning of their parameters, sensitivity analysis to approximate errors in predictive plotting is desired.

The performance criteria of the Kostiakov and the Philip models exhibited similar variations. Except for site 2, the *Nash* values from both models are similar, with a maximum range difference of 0.985 and 0.969 at site 18, respectively. Similar ascertainments are drawn from the values of *RMSE* with distinctive differences at site 2 and considerably moderate differences for sites 12, 18, 19, and 21. Nonetheless, while the *Bias* estimates for the Kostiakov model are found relatively in the range of −0.7 at site 24 and 0.3 at site 20, *Bias* for the Philp model was chaotic for all sites and ranged from −2.3 at site 2 to 0 at site 20. Therefore, it can be concluded that the next best model for the Madjez Ressoul Catchment is the Kostiakov model, but this cannot be generalized to all sites. It is worth noting that the parameters of the Philip model were adjusted at each time during the whole period of estimation.

Moreover, although parameter ***S*** of the Philip model reflects approximately the Sorptivity of the soil, parameter ***K*** was found as not closely dependent on the infiltration rate [80,81]. The inferior ability of the Philip model to accurately express infiltration rates for Madjez Ressoul Catchment suggests that the soil structure and other hydraulic parameters are crucial factors affecting infiltration. It can be concluded that the applicability of the Philip model for the Madjez Ressoul Catchment requires further site investigations and measurements on small grids to estimate its parameters experimentally, rather than using estimates from the model. It is also clear that site 2 (i.e., a superficial formation within a dry farming zone) and site 7 (i.e., a conglomerate soil) require further site investigations.

## 4. Conclusions

This study investigated the application of the three most renowned infiltration models to the semi-arid Madjez Ressoul catchment in Northern Algeria. The catchment is known as one of the few remaining natural catchments with respect to the diversity of the soil cover and its non-altered land use. In situ experimental measurements were carried out to cover the aerial extent of the catchment despite the complex relief and the difficulties encountered to include the higher ridges. The initial water contents were evaluated through laboratory tests from samples taken in the vicinity of the field measurements. The qualitative performance of the three models (i.e., Philips, Kostiakov, and Horton) was evaluated based on four statistical criteria: the *Nash*–Sutcliffe efficiency, correlation coefficient, Root mean square error, and *Bias*. Assessment of the performance of the models against these criteria revealed the important effect of soil moisture, and the initial and final infiltration measurements on the superiority of the Horton model for estimating the infiltration rates of the Madjez Ressoul catchment. The Kostiakov model could be seen as a complementary alternative to assess the infiltration rate at most evaluated sites. The study suggests further investigations to include soil structure along with other hydraulic parameters to improve

the estimation of the Philip parameters in arid catchments where similar soil types exhibited distinct responses.

**Author Contributions:** The study was designed by H.B., A.D. and T.M. A.D. conducted the field experiments. A.D., H.B. and T.M. conducted the model setup and performed the simulations. A.D., T.M. and H.B. performed the data analysis and wrote and reviewed the paper. All authors have read and agreed to the published version of the manuscript.

**Funding:** This research received no external funding.

**Institutional Review Board Statement:** Not applicable.

**Informed Consent Statement:** Not applicable.

**Data Availability Statement:** Not applicable.

**Conflicts of Interest:** The authors declare no conflict of interest. The funding sponsors had no role in the design of the study; in the collection, analyses, or interpretation of data; in the writing of the manuscript; or in the decision to publish the results.

## References

1. Davidsen, S.; Löwe, R.; Ravn, N.H.; Jensen, L.N.; Arnbjerg-Nielsen, K. Initial Conditions of Urban Permeable Surfaces in Rainfall-Runoff Models Using Horton's Infiltration. *Water Sci. Technol.* **2018**, *77*, 662–669. [CrossRef] [PubMed]
2. Guellouz, L.; Askri, B.; Jaffré, J.; Bouhlila, R. Estimation of the soil hydraulic properties from field data by solving an inverse problem. *Sci. Rep.* **2020**, *10*, 9359. [CrossRef] [PubMed]
3. Nartowska, E.; Kozłowski, T.; Gawdzik, J. Assessment of the influence of copper and zinc on the microstructural parameters and hydraulic conductivity of bentonites on the basis of SEM tests. *Heliyon* **2019**, *5*, e02142. [CrossRef] [PubMed]
4. Sakellariou-Makrantonaki, M.; Angelaki, A.; Evangelides, C.; Bota, V.; Tsianou, E.; Floros, N. Experimental Determination of Hydraulic Conductivity at Unsaturated Soil Column. *Procedia Eng.* **2016**, *162*, 83–90. [CrossRef]
5. Li, Y.; Shao, M. Effects of rainfall intensity on rainfall infiltration and redistribution in soil on Loess slope land. *Ying Yong Sheng Tai Xue Bao* **2006**, *17*, 2271–2276. [PubMed]
6. Tsai, Y.J.; Yeh, H.-f. Effect of variations in rainfall intensity and different return period rainfall events on unsaturated slope stability. *J. Taiwan Agric. Eng.* **2019**, *65*, 34–50. [CrossRef]
7. Lipiec, J.; Kuś, J.; Słowińska-Jurkiewicz, A.; Nosalewicz, A. Soil porosity and water infiltration as influenced by tillage methods. *Soil Tillage Res.* **2006**, *89*, 210–220. [CrossRef]
8. Sajjadi, S.-A.-H.; Mirzaei, M.; Nasab, A.F.; Sarkardeh, H. Effect of Soil Physical Properties on Infiltration Rate. *Geomech. Eng.* **2016**, *10*, 727–736. [CrossRef]
9. Barbosa, L.C.; de Souza, Z.M.; Franco, H.C.J.; Otto, R.; Rossi Neto, J.; Garside, A.L.; Carvalho, J.L.N. Soil texture affects root penetration in oxisols under sugarcane in Brazil. *Geoderma Reg.* **2018**, *13*, 15–25. [CrossRef]
10. Biswas, A. Joint multifractal analysis for three variables: Characterizing the effect of topography and soil texture on soil water storage. *Geoderma* **2019**, *334*, 15–23. [CrossRef]
11. Kalhoro, S.A.; Ding, K.; Zhang, B.; Chen, W.; Hua, R.; Hussain Shar, A.; Xu, X. Soil infiltration rate of forestland and grassland over different vegetation restoration periods at Loess Plateau in northern hilly areas of China. *Landsc. Ecol. Eng.* **2019**, *15*, 91–99. [CrossRef]
12. Hino, M.; Odaka, Y.; Nadaoka, K.; Sato, A. Effect of initial soil moisture content on the vertical infiltration process—A guide to the problem of runoff-ratio and loss. *J. Hydrol.* **1988**, *102*, 267–284. [CrossRef]
13. Schoener, G.; Stone, M.C. Impact of antecedent soil moisture on runoff from a semiarid catchment. *J. Hydrol.* **2019**, *569*, 627–636. [CrossRef]
14. Avellaneda, E. Infiltration through Roadside Swales. Master's Thesis, University of Central Florida, Orlando, FL, USA, 1985.
15. Neris, J.; Tejedor, M.; Rodríguez, M.; Fuentes, J.; Jiménez, C. Effect of forest floor characteristics on water repellency, infiltration, runoff and soil loss in andisols of Tenerife (Canary Islands, Spain). *CATENA* **2013**, *108*, 50–57. [CrossRef]
16. Pingping, H.; Xue, S.; Zhanbin, L. Effect of vegetation cover types on soil infiltration under simulating rainfall. *Nat. Environ. Pollut. Technol.* **2013**, *12*, 193–198.
17. Zhao, C.; Jia, X.; Zhu, Y.; Shao, M.A. Long-term temporal variations of soil water content under different vegetation types in the Loess Plateau, China. *CATENA* **2017**, *158*, 55–62. [CrossRef]
18. Rahman, M.A.; Moser, A.; Anderson, M.; Zhang, C.; Rötzer, T.; Pauleit, S. Comparing the infiltration potentials of soils beneath the canopies of two contrasting urban tree species. *Urban For. Urban Green.* **2019**, *38*, 22–32. [CrossRef]
19. Vieux, B.E. Infiltration modeling. In *Distributed Hydrologic Modeling Using GIS*; Water Science and Technology Library; Springer: Dordrecht, The Netherlands, 2004; Volume 48, pp. 91–113. [CrossRef]
20. Fox, D.M.; Bryan, R.B.; Price, A.G. The influence of slope angle on final infiltration rate for interrill conditions. *Geoderma* **1997**, *80*, 181–194. [CrossRef]

21. Chatterjee, D.; Murali Krishna, A. Effect of slope angle on the stability of a slope under rainfall infiltration. *Indian Geotech. J.* **2019**, *49*, 708–717. [CrossRef]
22. Patle, G.T.; Sikar, T.T.; Rawat, K.S.; Singh, S.K. Estimation of infiltration rate from soil properties using regression model for cultivated land. *Geol. Ecol. Landsc.* **2019**, *3*, 1–13. [CrossRef]
23. Sihag, P.; Tiwari, N.K.; Ranjan, S. Support vector regression-based modeling of cumulative infiltration of sandy soil. *ISH J. Hydraul. Eng.* **2020**, *26*, 44–50. [CrossRef]
24. Sihag, P.; Kumar, M.; Sammen, S.S. Predicting the infiltration characteristics for semi-arid regions using regression trees. *Water Supply* **2021**, *21*, 2583–2595. [CrossRef]
25. Cortes-D, D.L.; Camacho-Tamayo, J.H.; Giraldo, R. Spatial prediction of soil infiltration using functional geostatistics. *AUC Geogr.* **2018**, *53*, 149–155. [CrossRef]
26. Mishra, S.K.; Tyagi, J.V.; Singh, V.P. Comparison of Infiltration Models. *Hydrol. Process.* **2003**, *24*, 2629–2652. [CrossRef]
27. Zakwan, M.; Muzzammil, M.; Alam, J. Application of spreadsheet to estimate infiltration parameters. *Perspect. Sci.* **2016**, *8*, 702–704. [CrossRef]
28. Sihag, P.; Tiwari, N.K.; Ranjan, S. Estimation and intercomparison of infiltration models. *Water Sci. Technol.* **2017**, *31*, 34–43. [CrossRef]
29. Singh, B.; Sihag, P.; Singh, K. Comparison of infiltration models in NIT. Kurukshetra Campus. *Appl. Water Sci.* **2018**, *9*, 63. [CrossRef]
30. Vand, A.S.; Sihag, P.; Singh, B.; Zand, M. Comparative evaluation of infiltration models. *KSCE J. Civ. Eng.* **2018**, *22*, 4173–4184. [CrossRef]
31. Farid, H.U.; Mahmood-Khan, Z.; Ahmad, I.; Shakoor, A.; Anjum, M.N.; Iqbal, M.M.; Mubeen, M.; Asghar, M. Estimation of infiltration models parameters and their comparison to simulate the onsite soil infiltration characteristics. *Int. J. Agric. Biol. Eng.* **2019**, *2*, 84–91.
32. Ebrahimian, H.; Ghaffari, P.; Ghameshlou, A.N.; Tabatabaei, S.-H.; Alizadeh Dizaj, A.A. Extensive comparison of various infiltration estimation methods for furrow irrigation under different field conditions. *Agric. Water Manag.* **2020**, *230*, 105960. [CrossRef]
33. Ramesh, V.B.; Bandhyopadhyay, K.K.; Sharma, K.L.; Bhattacharyya, T.; Wani, S.P. Land use and soil management effects on infiltration model parameters in semi-arid tropical alfisols. *Ann. Arid. Zone* **2010**, *49*, 1–8.
34. Horton, R.E. Analysis of runoff-plat experiments with varying infiltration-capacity. *Eos. Trans. Am. Geophys. Union* **1939**, *20*, 693–711. [CrossRef]
35. Holtan, H.N. *A Concept of Infiltration Estimates in Watershed Engineering*; ARS (Series) Agricultural Research Service 41–51; U.S. Department of Agriculture: Washington, DC, USA, 1961; pp. 1–32.
36. Bauer, S.W. A modified Horton equation for infiltration during intermittent rainfall. *Hydrol. Sci. Bull.* **1974**, *19*, 219–225. [CrossRef]
37. Gabellani, S.; Silvestro, F.; Rudari, R.; Boni, G. General calibration methodology for a combined Horton-SCS infiltration scheme in flash flood modeling. *Nat. Hazards Earth Syst. Sci.* **2008**, *8*, 1317–1327. [CrossRef]
38. Verma, S.C. Modified Horton's infiltration equation. *J. Hydrol.* **1982**, *58*, 383–388. [CrossRef]
39. Akan, A.O. Horton Infiltration Equation revisited. *J. Irrig. Drain. Eng.* **1992**, *118*, 828–830. [CrossRef]
40. Esen, I.I.; Almedeij, J. Generalized Horton Model for Low-Intensity rainfall. *Soil Sci.* **2013**, *178*, 174–179. [CrossRef]
41. Green, I.R.A. An explicit solution of the modified Horton equation. *J. Hydrol.* **1986**, *83*, 23–27. [CrossRef]
42. Aron, G. Adaptation of Horton and SCS infiltration equations to complex storms. *J. Irrig. Drain. Eng.* **1992**, *118*, 275–284. [CrossRef]
43. Arnold, J.G.; Allen, P.M.; Bernhardt, G. A comprehensive surface-groundwater flow model. *J. Hydrol.* **1993**, *142*, 47–69. [CrossRef]
44. Diskin, M.H.; Nazimov, N. Linear reservoir with feedback regulated inlet as a model for the infiltration process. *J. Hydrol.* **1995**, *172*, 313–330. [CrossRef]
45. Ottoni Filho, T.B.O.; Ottoni, M.V.; Oliveira, M.B.; Macedo, J.R. Estimation of field capacity from ring infiltrometer-drainage data. *Rev. Bras. Ciênc. Solo* **2014**, *38*, 1765–1771. [CrossRef]
46. Razzaghi, S.; Khodaverdiloo, H.; Dashtaki, S.G. Effects of long-term wastewater irrigation on soil physical properties and performance of selected infiltration models in a semi-arid region. *Hydrol. Sci. J.* **2016**, *61*, 1778–1790. [CrossRef]
47. Li, M.; Liu, T.; Duan, L.; Luo, Y.; Ma, L.; Zhang, J.; Zhou, Y.; Chen, Z. The scale effect of double-ring infiltration and soil infiltration zoning in a semi-arid steppe. *Water* **2019**, *11*, 1457. [CrossRef]
48. Mbagwu, J.S.C. *Analysis of Physical Properties Controlling Steady-State Infiltration Rates on Tropical Savannah Soils*; IC—93/289; International Atomic Energy Agency: Vienna, Austria, 1993; Volume 25, pp. 1–11.
49. Askari, M.; Tanaka, T.; Setiawan, B.I.; Saptomo, S.K. Infiltration characteristics of tropical soil based on water retention data. *J. Jpn Soc. Hydrol. Water Resour.* **2008**, *21*, 215–227. [CrossRef]
50. Suryoputro, N.; Soetopo, W.; Suhartanto, E.S.; Limantara, L.M. Evaluation of infiltration models for mineral soils with different land uses in the tropics. *J. Water Land Dev.* **2018**, *37*, 153–160. [CrossRef]
51. Bach, L.B.; Wierenga, P.J.; Ward, T.J. Estimation of the Philip Infiltration Parameters from Rainfall Simulation Data. *Soil Sci. Soc. Am. J.* **1986**, *50*, 1319–1323. [CrossRef]
52. Mahapatra, S.; Jha, M.K.; Biswal, S.; Senapati, D. Assessing variability of infiltration characteristics and reliability of infiltration models in a tropical sub-humid region of India. *Sci. Rep.* **2020**, *10*, 1515. [CrossRef] [PubMed]

53. Oku, E.; Aiyelari, A. Predictability of Philip and Kostiakov infiltration models under inceptisols in the humid forest zone, Nigeria. *Kasetsart J. Nat. Sci.* **2011**, *45*, 594–602.
54. Utin, U.E.; Oguike, P.C. Evaluation of Philip's and Kostiakov's infiltration models on soils derived from three parent materials in Akwa Ibom state, Nigeria. *J. Sci. Eng. Res.* **2018**, *5*, 79–87.
55. Zolfaghari, A.A.; Mirzaee, S.; Gorji, M. Comparison of different models for estimating cumulative infiltration. *Int. J. Soil Sci.* **2012**, *7*, 108–115. [CrossRef]
56. Zakwan, M. Assessment of dimensionless form of Kostiakov model. *Aquademia Water Environ. Technol.* **2017**, *1*, 1. [CrossRef]
57. Jagani, A.H.; Shrivastava, P.K.; Dwivedi, D.K. Evaluation of Kostiakov's and Philip's infiltration models on the soil of Dediapada, India. *India J. Appl. Nat. Sci.* **2018**, *10*, 1073–1077. [CrossRef]
58. Igboekwe, M.U.; Adindu, R.U. Use of Kostiakov's infiltration model on Michael Okpara University of Agriculture, Umudike soils, Southeastern, Nigeria. *Water Resour. Prot.* **2014**, *6*, 888–894. [CrossRef]
59. Lei, G.; Fan, G.; Zeng, W.; Huang, J. Estimating parameters for the Kostiakov-Lewis infiltration model from soil physical properties. *J. Soils Sediments* **2020**, *20*, 166–180. [CrossRef]
60. Thomas, A.; Ofosu, A.; Emmanuel, A.; De-Graft, A.; Ayine, A.; Asare, A.; Alexander, A. Comparison and Estimation of Four Infiltration Models. *Open J. Soil Sci.* **2020**, *10*, 45–57. [CrossRef]
61. Ogbe, V.B.; Jayeoba, O.J.; Ode, S.O. Comparison of four soil infiltration models on a sandy soil in Lafia, Southern Guinea Savanna zone of Nigeria. *Prod. Agric. Technol.* **2011**, *7*, 116–126.
62. Mohamoud, Y.M. Evaluating the green and αMPT infiltration parameter values for tilled and crusted soils. *J. Hydrol.* **1991**, *123*, 25–38. [CrossRef]
63. Adindu, R.; Igbokwe, K.; Chigbu, T.; Ike-Amadi, C. Application of Kostiakov's infiltration model on the soils of umudike, Abia state—Nigeria. *Am. J. Environ. Eng.* **2014**, *4*, 1–6.
64. Rahmati, M.; Weihermüller, L.; Vanderborght, J.; Pachepsky, Y.A.; Mao, L.; Sadeghi, S.H.; Moosavi, N.; Kheirfam, H.; Montzka, C.; Van Looy, K.; et al. Development and analysis of the Soil water Infiltration Global database. *PANGAEA* **2018**, *10*, 1237–1263. [CrossRef]
65. Zadjaoui, A. Numerical modelling of infiltration profiles in the silt Tlemcen (Algeria). *E3S Web Conf.* **2016**, *9*, 11015. [CrossRef]
66. Smail, A.S.; Bouheraoua, A.; Abdesselam, M. Caractérisation hydrodynamique des sols de la haute vallée de l'oued Sébaou (Algérie): Étude expérimentale, numérique et analytique. *Phys. Géo* **2013**, *7*, 261–283. [CrossRef]
67. Boers, T.M.; van Deurzen, F.J.M.P.; Eppink, L.A.A.J.; Ruytenberg, R.E. Comparison of infiltration rates measured with an infiltrometer, a rainulator and a permeameter for erosion research in SE Nigeria. *Soil Technol.* **1992**, *5*, 13–26. [CrossRef]
68. Akinbile, C. Comparative analysis of infiltration measurements of two irrigated soils in Akure, Nigeria. *Adv. Appl. Sci. Res.* **2010**, *1*, 49–57.
69. Mavimbela, S.S.W.; van Rensburg, L.D. Characterizing infiltration and internal drainage of South African dryland soils. *Earth Surf. Process. Landf.* **2017**, *42*, 414–425. [CrossRef]
70. Lasisip, M.O.; Bof, P.; Awe, B.S. Assessment of infiltration capacity of agricultural soil in Ado-Ekiti southwestern Nigeria using selected empirical models. *Int. J. Innov. Sci. Eng. Technol.* **2017**, *4*, 111–117.
71. Ehiomogue, P.; Ojedele, O.S.; Ikechuchu-Ede, C.E.; Okosa Iorji, F.N.; Ahaneku, I.E. Calibration of existing infiltration models on different amended soils. *Am. J. Eng. Res.* **2018**, *7*, 242–247.
72. Robinson, A.R.; Rohwer, C. Measurement of canal seepage. *Trans. ASCE* **1957**, *122*, 347–363.
73. Weiler, M.; Naef, F. An experimental tracer study of the role of macropores in infiltration in grassland soils. *Hydrol. Process.* **2003**, *17*, 477–493. [CrossRef]
74. Horton, R.E. An approach toward a physical interpretation of infiltration-capacity. *Soil Sci. Soc. Am. J.* **1941**, *5*, 399–417. [CrossRef]
75. Beven, K.; Robert, E. Horton's perceptual model of infiltration processes. *Hydrol. Process.* **2004**, *18*, 3447–3460. [CrossRef]
76. Kostiakov, A.N. The dynamics of the coefficients of water percolation in soils and the necessity for studying it from a dynamic point of view for purpose of amelioration. *Soc. Soil Sci.* **1932**, *14*, 17–21.
77. Philip, J.R. The theory of infiltration: 1. The infiltration equation and its solutions. *Soil Sci.* **1957**, *83*, 345–358. [CrossRef]
78. Monroe, J.S.; Wicander, R. *The Changing Earth: Exploring Geology and Evolution*, 5th ed.; Brooks Cole: Salt Lake City, UT, USA, 2008; p. 735.
79. Ghosh, R.K. A note on Lewis-Kostiakov's infiltration equation. *Soil Sci.* **1985**, *139*, 193–196. [CrossRef]
80. Philip, J.R. Theory of Infiltration. *Adv. Hydrosci.* **1969**, *5*, 215–296. [CrossRef]
81. Sir, M.; Kutilek, M.; Kuraz, V.; Krejca, M.; Kubik, F. Field estimation of the soil hydraulic characteristics. *Soil Technol.* **1988**, *1*, 63–75. [CrossRef]